

# Solubility Analysis of Pharmaceuticals Guaifenesin, Ketoprofen, and Artemisinin in Different Solvents

Masoud Sadeghi<sup>1\*</sup>, Francesca Cascella<sup>1</sup>, Vico Tenberg<sup>1</sup>, Andreas Seidel-Morgenstern<sup>1,2</sup>  
and Heike Lorenz<sup>1</sup>

<sup>1</sup>Max Planck Institute for Dynamics of Complex Technical Systems, Magdeburg,  
Germany

<sup>2</sup>Otto-von-Guericke-University Magdeburg, Institute of Process Engineering, Chair  
for Chemical Process Engineering, Magdeburg, Germany

---

Corresponding author. Tel.: +49 391 6110 321; E-mail address:  
sadeghi@mpi-magdeburg.mpg.de (M. Sadeghi).

## **Abstract**

Solubility is a fundamental parameter in the discovery of new drug molecules as well as in their production using crystallization processes. In this work, we experimentally investigate the solubility in different solvents and the density of the anti-cough drug guaifenesin and characterize its solid state via Powder X-Ray Diffraction (PXRD) and thermal analysis. Moreover, a strategy is developed and successfully applied to predict the density and solubility behavior of that pharmaceutical. On the solubility curve concentration and temperature depend on each other for a binary solution at fixed pressure. Therefore, densities of undersaturated aqueous solutions of guaifenesin are measured and used alongside with solubility data to obtain more realistic parameters of thermodynamic model. Perturbed Chain-Statistical Associating Fluid Theory (PC-SAFT) Equation of State (EoS) is used. It was able to successfully represent the solubility curves using a small amount of data for fitting the model parameters. In a second part, the applicability of the model to predict the solubility in various organic solvents of two other pharmaceutically relevant molecules, namely the anti-inflammatory drug ketoprofen and the antimalarial compound artemisinin has been studied.

The results showed that guaifenesin is the most soluble in ethanol and least soluble in ethyl acetate. Its aqueous solubility shows a special behavior with a specific sharp increase with temperature. In all of the solvents, ketoprofen is the highest soluble among the compounds studied followed by guaifenesin and artemisinin. PC-SAFT is able to capture the experimentally observed effects of temperature, and solvent type on the solubility behavior of each of the three solutes.

**Keywords:** Solubility; Density; Guaifenesin; Thermal analysis; PC-SAFT

## 1. Introduction

Crystallization is one of the most important separation methods that widely used in pharmaceutical industry. In each crystallization process, target molecules must be separated from impurities. This is especially important in the case of pharmaceuticals as small amounts of impurities may cause severe health-related problems. Therefore, efficient crystallization processes and their rational design are of pivotal importance for pharma industries.

The solubility of medicinal molecules is a pronounced concern in the pharmaceutical field to detect and develop new drug candidates. It is a key parameter widely used in many stages of the drug discovery to evaluate the quality of a drug candidate in terms of its oral absorption, metabolism, distribution and toxicity. In drug development, solubility is a crucial attribute with respect to designing experiments to identify potential salts, cocrystals, polymorphic forms, solvates and hydrates as well as developing analytical procedures [DiL12]. Moreover, solubility of pharmaceutical molecules is a crucial parameter affecting the drug functionality in the body. Consequently, solubility of drug molecules and the effect of different operational conditions like temperature as well as solvents on their solubility should be taken into account.

Theoretical as well as experimental studies have been directed towards the understanding of solubility behavior of pharmaceuticals. Solubility determination can be carried out experimentally using various techniques such as gravimetry[Sot20], spectroscopy[Lin09], thermal[Ras18], microscopy[Yan11] and laser [HeH21] analysis. Empirical [2, 8, 9], semi-empirical (NRTL-SAC[Che04], UNIQUAC[Mir06]; UNIFAC[13-15], Mod-UNIFAC[Die11]) and theoretical-based models (modern equations of states such as SAFT-based[Rüt09] or COSMO-based

models[Bou11]) are widely used in the literature to model the solubility curves of the pharmaceutical components. Despite these efforts, solubility of many drug molecules in a wide range of solvents and operational conditions are still scarce. Furthermore, in the early development steps of pharmaceuticals, there is a little amount of that component available[Bou11] with a high price. Therefore, having a model to at least qualitatively predict the solubility is valuable. However, as pharmaceuticals are usually complex molecules with different functional groups and many flexible conformations, estimation of the solubility using the current models is a challenging task and deserves much more efforts. An important issue regarding the current models is the way in which the model parameters are obtained. A widely used method is to fit the adjustable parameters of the model to the solubility data. However, on the solubility curve of a typical pharmaceutical in a solvent, temperature and concentration depend on each other at fixed pressure. Hence, fitting the model to just one solubility curve, does not separately account for the effect of temperature and concentration on the model-parameters [8].

Based on the above-mentioned arguments, we follow a two-fold goal in the current article. In the experimental section, we aim to investigate the solubility behavior of guaifenesin. It is an antitussive agent widely used as expectorant in many cough suppressive formulations as well as for respiratory tract infections and bronchitis. Guaifenesin is an ether of guaiacol, a constituent of guaiac resin from the wood of *Guajacum officinale* Linne,[Dic09] and it is chemically 3-(2-methoxyphenoxy)propane-1,2-diol (Fig. 1a).

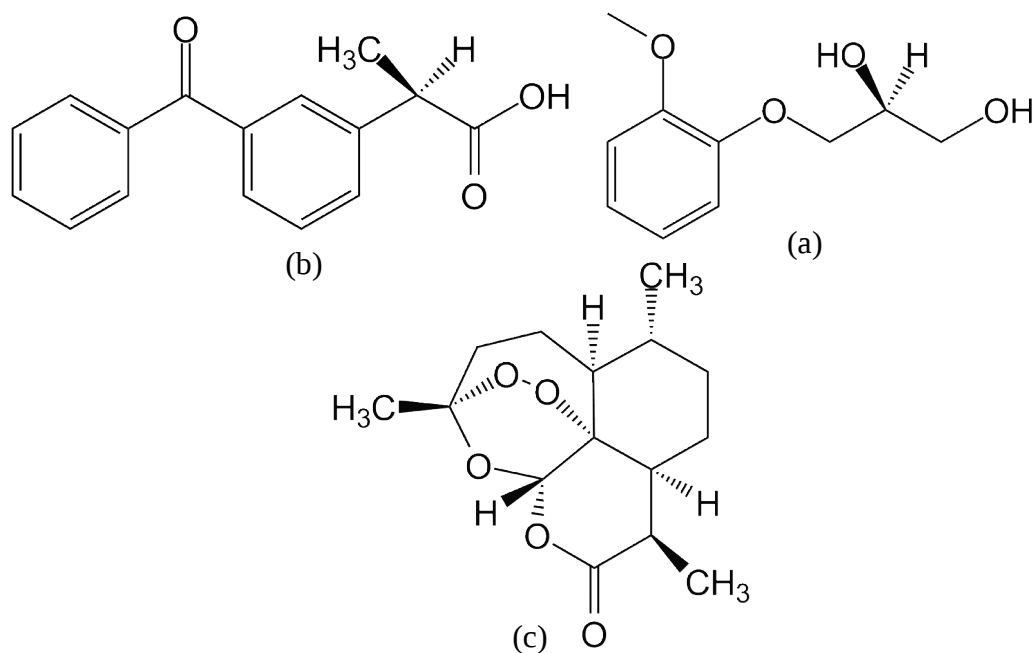


**Fig. 1.** Molecular structure of (a): 3- (2-methoxyphenoxy) -propane-1, 2-diol (guaifenesin), (b): 2-(3-benzoylphenyl)-propionic acid (ketoprofen) and (c): artemisinin.

Guaifenesin has gained much attention in the scientific community, not only as cough medication but also due to its enhanced therapeutic effect when combined with non-steroidal anti-inflammatory drugs (NSAIDs) in the treatment of common cold. The co-administration of medication for cough and pain relievers is a common procedure to alleviate the symptoms of the common cold and in this scenario the API guaifenesin has been found to influence the adsorption of paracetamol and NSAIDs such as ibuprofen and nimesulide[Mah14].

In the literature, beside our own data there are few investigations of the solubility and thermal behavior of guaifenesin [23-25]. However, and to the best of our knowledge, this work is the first systematic report of the solubility behavior of guaifenesin in different solvents in the open literature. In addition, we study density, heat capacity and solid form of guaifenesin using pycnometric, DSC (Differential Scanning Calorimetry) and PXRD methods. Using racemic guaifenesin in this study, we simply refer to the molecule as guaifenesin throughout the paper.

In the theoretical section, we present a strategy to model the solubility using a state-of-the-art EoS, namely PC-SAFT. We use PC-SAFT to model the experimental data of solubility and density. In addition, we expand the modelling to represent the solubility of ketoprofen and artemisinin as respectively chiral anti-inflammatory and antimalarial drugs (Fig. 1b and c)[Sot20].

The structure of the paper is as follows: in the experimental section, materials, measurement methods and analysis techniques are given. The basic equations of the solubility modelling and PC-SAFT EoS are included in the theoretical section. The results of our experimental work for guaifenesin and the modelling of guaifenesin, ketoprofen, and artemisinin are presented and discussed in the results and discussion section. Finally, a summary and outlook for the future work are given.

## 2. Experimental section

### 2.1. Materials

Guaifenesin, guaiacol glycerol ether, was purchased from TCI Deutschland GmbH. The chemical purity of the substance was above 98 % and was used without further treatment. The organic solvents used for solubility measurements were purchased from VWR International. The details of the materials used in this work are summarized in Table 1.

Table 1: Detailed information of the chemicals used in this work

Material	CAS	Source	Purity	Molar mass (g/mol)
Guaiacol glycerol ether	93-14-1	TCI Chemicals	>98 % (HPLC)	198.22
2-Propanol	67-63-0	VWR International	≥99.8 %	60.10
Ethyl acetate	141-78-6	VWR International	≥99.8 %	88.11
Acetone	67-64-1	VWR International	≥99.8 %	58.08
Ethanol	64-17-5	VWR International	≥99.8 %	46.07

## *2.2. Calorimetric analysis*

DSC measurements were performed with a DSC 131 Setaram (France), calibrated with pure metals (indium, tin, lead), under pure helium atmosphere. Moreover, DSC 111 Setaram (France), under nitrogen gas flow was used for heat capacity measurements. Samples of 6-7 mg of solid guaifenesin were prepared for the determination of its melting temperature, while for heat capacity measurements samples of  $\approx 50$  mg were used. The onset temperature of the DSC thermograms is considered as the melting point and the melting enthalpy is calculated using the area below the curve. All of the experiments were repeated twice and the standard deviation is calculated.

## *2.3. PXRD analysis*

PXRD measurements were aimed to identify the solid-state form of the solid in equilibrium with the saturated solutions at various temperatures and in different solvents. Samples of 1 mL of the equilibrated suspensions were withdrawn and each suspension was then filtrated. The isolated solid phases were washed with the corresponding solvent of the solubility measurements and used for PXRD analysis. An X'Pert Pro diffractometer (PANalytical GmbH, Germany) was used, with radiation  $\text{CuK}\alpha$ ,  $2\theta$  range between 3 and  $40^\circ$ , resolution step  $0.017^\circ$  and 50 s of counting time for each step.

## *2.4. Liquid and particle density determination*

An off-line DM-40 Mettler Toledo density meter was used to determine the density of various undersaturated as well as saturated solutions of racemic guaifenesin in

different pure and mixed solvents. Based on the solubility data previously determined, various solutions were prepared and injected into the densitometer cell and the density is measured at specific temperatures. Also, two replicates of the density-measurements were performed.

A pycnometer has been used to determine the solid density of one of the studied systems, i.e. racemic guaifenesin. After determining the mass of the pycnometer, solid guaifenesin has been introduced into the device up to two third of its volume and the mass of the pycnometer with the solid has been determined. Then the pycnometer has been filled with a solvent in which guaifenesin is completely insoluble, in this case methyl tert-butyl ether (MTBE) and covered with its appropriate capillary cap. Afterwards, the total mass with the added solvent has been determined. The solid density of guaifenesin has been calculated using Eq. (1):

$$\rho_{solid} = \frac{m_2 - m_1}{V_1 - \left(\frac{m_3}{\rho_3}\right)} \quad (1)$$

Where,  $m_1$  is the mass of the empty pycnometer,  $m_2$  is the mass of the pycnometer filled with solid guaifenesin,  $m_3$  is the mass of MTBE,  $\rho_3$  is the density of MTBE and  $V_1$  is the total volume of the pycnometer.

### 2.5. Solubility measurements

The solubility of guaifenesin in various organic solvents was determined using an isothermal method. The measurements consisted of preparing suspensions of the chiral system in a chosen solvent in sealed vials. The vials equipped with a magnetic stirrer were immersed in a water bath within double-jacketed vessels connected to a thermostat. Especially, sealed vials of 20 mL volume were used. A Pt-100 probe was used to monitor the temperature with the time. Several temperatures were investigated

between 283.15 and 333.15 K. The suspensions were thermally equilibrated over 48 h under continuous stirring in order to ensure a homogeneous mixing. The equilibration and the achievement of the saturation concentration were verified by observing the variation of the concentration with the time. Gravimetric analysis allowed to determine the concentration of the saturated solutions,  $\omega_{sat.}(T)$ . A sample of 1 mL of the suspension was withdrawn and filtrated; hence, the saturation concentrations were derived as expressed by Eq. (2):

$$\omega_{sat.}(T) = \frac{m_{solute}}{m_{solute} + m_{solvent}} \quad (2)$$

Where  $m_{solute}$  is the mass of the solute that remained after complete evaporation of the solvent. Between two and six replicates of the measurements were carried out at each temperature and for each solvent, in order to determine the standard deviations of the final concentration values.

### 3. Theoretical section

At the thermodynamic equilibrium, the chemical potential of the solute in the solid phase equals that of the solute in the solution. Chemical potentials can be expressed in terms of the activities and choosing the melt as the reference state leads to the following equality [Pra99]:

$$\ln (a_{\text{pure solid}}) = \ln (a^{\text{solute} \in \text{the liquid phase}}) = \ln (x) + \ln (\gamma) \quad (3)$$

Where,  $a$ ,  $x$  and  $\gamma$  are respectively, activity, solubility and activity coefficients. Here, we are considering systems in which a pure solid phase is in equilibrium with a liquid solution. Hence, activity of a pure solid should be calculated. This parameter can be expressed in terms of the thermal data using a thermodynamic cycle [Pra99]:

$$\ln (a_{\text{pure solid}}) = \frac{-\Delta H_m(T_m)}{RT} \left(1 - \frac{T}{T_m}\right) - \frac{1}{RT} \int_{T_m}^T \Delta C_{p,m} dT + \frac{1}{R} \int_{T_m}^T \frac{\Delta C_{p,m}}{T} dT \quad (4)$$

$\Delta H_m$ ,  $T_m$ ,  $R$ ,  $T$  and  $C_{p,m}$  are molar melting enthalpy, melting temperature, gas constant, temperature, and molar heat capacity, respectively.  $\Delta C_{p,m}$  is the difference between the molar heat capacity of the melt ( $C_{p,m}^{\text{pure melt}}$ ) and the molar heat capacity of the solid ( $C_{p,m}^{\text{pure solid}}$ ) [CITATION Sad 191 [8]] :

$$\Delta C_{p,m} = C_{p,m}^{\text{pure melt}} - C_{p,m}^{\text{pure solid}} \quad (5)$$

In order to model the solubility data, in addition to the calculation of the activity of the solid (Eq. (4)), the activity coefficient of the solute in the solution should be determined. Activity coefficients account for different interactions inside the solution. In fact, at a fixed physical condition (temperature and pressure) the activity of a pure

solid is fixed. However, its solubility in two different solvents is generally not the same. Activity coefficients are the only parameters that enable us to distinguish between the solubility of a specific solid in two different solvents. Hence, they must be taken into account for an accurate solubility modelling. Consequently, it is of crucial importance to have a reliable model for the calculation of activity coefficients. From the fundamentals of thermodynamics, activity coefficients are related to the osmotic coefficients:

$$\ln(\gamma_i) = \ln(\varphi_i) - \ln(\varphi_i^{pure}) \quad (6)$$

$\varphi_i$  is the fugacity coefficient of component  $i$  in the liquid mixture and  $\varphi_i^{pure}$  is the fugacity coefficient of pure  $i$ . Therefore, an EoS can be used to calculate the osmotic coefficients and subsequently activity coefficients of the molecules in the solution are determined. In this work a theoretically based EoS, namely PC-SAFT[Gro01], was used to calculate activity coefficients. This model obtained using statistical thermodynamic fundamentals [32-36]. In addition, it is a flexible model regarding the modelling of different classes of molecules [37-43]. In this regard, solubility and phase diagram calculations of pharmaceuticals are two crucial aspects captured using PC-SAFT [44-46]. This EoS considers molecules to be chains of spherically connected segments. These chains of segments interact with each other through repulsive, dispersive or directional (e.g. hydrogen bond formation) forces. A schematic model representation of an aqueous mixture containing guaifenesin is depicted in Fig. 2.

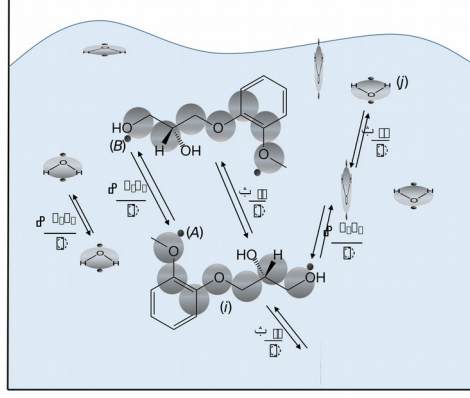


**Fig. 2.** Schematic representation of the interaction between guaifenesin (*i*) and water (*j*) molecules used for the calculations with PC-SAFT.

In this model each molecule is represented by segment number ( $m$ ), segment diameter ( $\sigma$ ) and dispersion energy interaction parameter  $\left(\frac{u}{k}\right)$ . For the molecules with the hydrogen bonding ability (e.g. water or guaifenesin) two other parameters,

namely association energy  $\left(\frac{\varepsilon^{A_i B_i}}{k}\right)$  and association volume  $(\kappa^{A_i B_i})$  should be considered. For associating systems, this work uses the number of association sites  $N_{association}=2$ . In order to describe the mixture properties from the pure component systems the following mixing rules should be considered[Gro01]:

$$\sigma_{ij} = \frac{\sigma_{ii} + \sigma_{jj}}{2} \quad (7)$$

$$\left(\frac{u}{k}\right)_{ij} = (1 - k_{ij}) \sqrt{\left(\frac{u}{k}\right)_{ii} \left(\frac{u}{k}\right)_{jj}} \quad (8)$$

$$\frac{\varepsilon^{A_i B_i}}{k} = 0.5 \left( \frac{\varepsilon^{A_i B_i}}{k} + \frac{\varepsilon^{A_j B_j}}{k} \right) \quad (9)$$

$$\kappa^{A_i B_i} = \left( \frac{\sqrt{\sigma_{ii} \sigma_{jj}}}{\sigma_{ij}} \right)^3 \sqrt{\kappa^{A_i B_i} \kappa^{A_j B_j}} \quad (10)$$

Therefore, each pure component  $i$  can be described using three (for non-associating molecules) or five (for associating molecules) physically sound parameters. Also, in a mixture of  $i$  and  $j$  molecules, the parameters can be determined using the above-mentioned mixing rules.  $k_{ij}$  is a binary adjustable parameter which corrects for the geometric mean assumption in the dispersion energy parameter.

Each type of interaction has a share in the thermodynamic properties calculated using PC-SAFT. This is an outcome of the underlying perturbation theory in which this model is based on. In this theory, all of the interactions which cause the non-ideality in the solution are additive and they can be summed up. Therefore, the compressibility factor ( $Z$ ) that accounts for deviation from ideal behavior is the summation of different contributions representing each kind of interactions given by [Gro01]:

$$Z = 1 + Z^{hard\ chain} + Z^{dispersion} + Z^{association} \quad (11)$$

Where  $Z^{hard\ chain}$  is the contribution due to the formation of chains from spherical segments,  $Z^{dispersion}$  and  $Z^{association}$  account respectively for dispersive and directional forces. Having the compressibility factor at hand, fugacity coefficient is calculated as follows [Cha90]:

$$kT \ln(\phi_i) = \mu_i^{res} - kT \ln(Z) \quad (12)$$

In Eq. (12)  $k$  is Boltzmann's constant and  $\mu_i^{res}$  is the residual chemical potential of molecule  $i$  in the solution. All of the expressions for the calculation of the different contributions to the compressibility factor and residual chemical potential are given in the related literature [30, 36].

## 4. Results and Discussions

### 4.1. Thermal analysis

DSC experiments were carried out to determine the melting temperature, melting enthalpy and heat capacity of guaifenesin. An endothermic peak at  $78.7 \pm 0.1$  °C was observed from the DSC thermogram, as shown in Fig. 3 and a melting enthalpy of  $217.5 \pm 0.5$  J g<sup>-1</sup> was determined. Melting temperature is in agreement with the previously published data, however, melting enthalpy differs ~15% [Bre06]. The thermal data of ketoprofen and artemisinin are also given in the Table 2 for the sake of completeness [Sot20]. Melting data of artemisinin were measured in our group and reported in Table 2 for the sake of completeness [Hor14]. However, PC-SAFT parameters are obtained using thermal data reported in the literature [Nti10], and we use these data for a fair comparison.

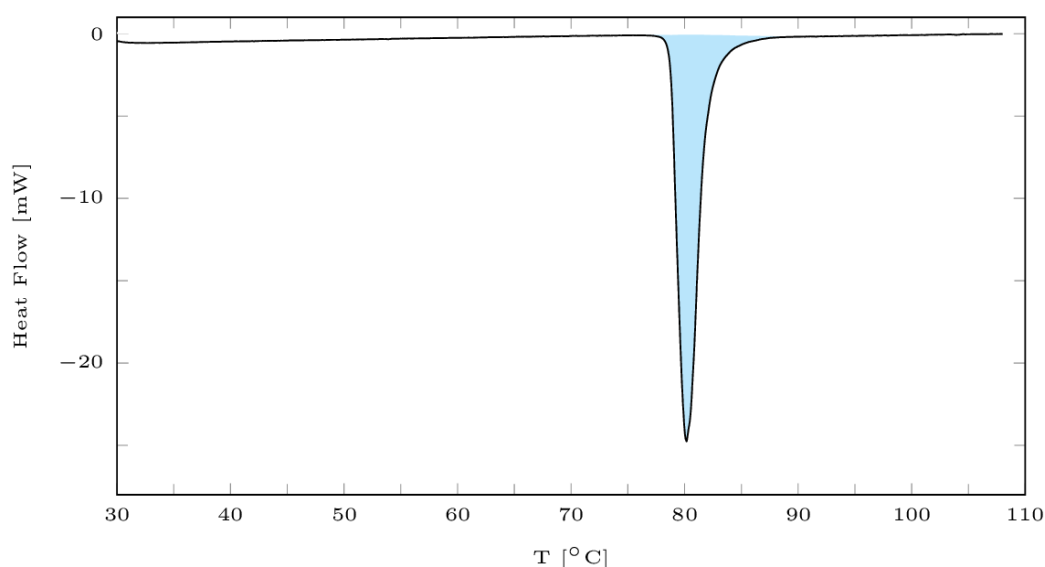


**Fig. 3.** DSC curve of guaifenesin showing its melting characteristics

**Table 2.** Thermal data of different pharmaceuticals used in this work

Reference	$\Delta C_{p,m} (JK^{-1}g^{-1})$	$T_m (K)$	$\Delta H_m (Jg^{-1})$	Component
This work	0.83	351.85	217.5	Guaifenesin
[Nti10]	0.20*	429.6	86.07	Artemisinin
[Hor14]	0.18*	424.6	78.4	
[Sot20]	0.31*	366.96	112.08	Ketoprofen

\*  $\Delta C_{p,m}$  is calculated using  $\Delta H_m/T_m$ .

Heat capacity data for solid as well as molten guaifenesin are reported in Table 3 and depicted in Fig. 4. Heat capacities are increasing with the increase of temperature. Also, due to more degrees of freedom, the heat capacity of the melt is higher than that of the solid phase. As the temperature reaches the melting point of guaifenesin,  $C_p$  increases sharply. This is the characteristics of a so-called first order phase transition in which heat capacity goes to infinity at the melting point.

**Table 3.** Experimental specific heat capacity data of guaifenesin and the corresponding standard deviation (S.D.)

$C_p \pm S.D. (JK^{-1}g^{-1}), melt$	$C_p \pm S.D. (JK^{-1}g^{-1}), solid$	$T (K)$
-	1.326±0.002	299.17
-	1.37±0.01	306.19
-	1.40±0.02	313.19
-	1.442±0.005	320.19
-	1.452±0.003	327.18
-	1.515±0.004	334.18
-	1.509±0.006	341.17
-	1.85±0.07	348.17
2.46±0.02	-	362.16
2.438±0.003	-	369.16
2.478±0.005	-	376.16
2.50±0.02	-	383.16
2.486±0.005	-	390.15

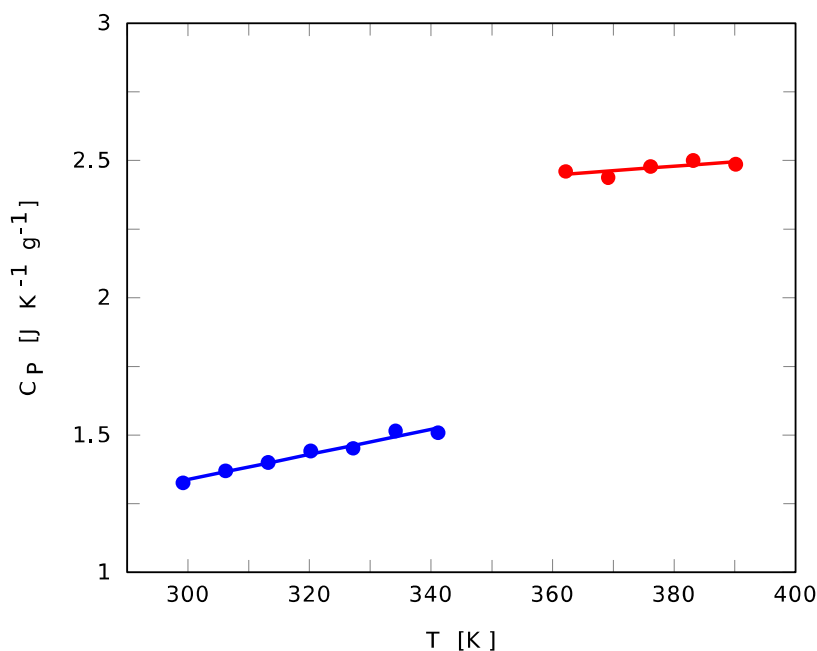


**Fig. 4.** Specific heat capacity of guaifenesin as a function of temperature (blue color for the solid and red color for the melt, dotted lines are added as a guide for the eyes)

Extrapolating of the solid and melt  $C_p$  data to the melting point, we approximately found that  $\Delta C_{p,m} = 0.83 J K^{-1} g^{-1}$ . This value is roughly 30% different from the

common approximation of  $\Delta C_{p,m} = \frac{\Delta H_m}{T_m} = 0.62 J K^{-1} g^{-1}$ . The DSC curve shows that there is no solid phase transition for guaifenesin before the endothermic peak. This is also confirmed using PXRD measurements that are presented in the next section.

#### 4.2. PXRD analysis

As shown in Fig. 5, the PXRD patterns of the solid phases in equilibrium with the saturated solutions in the organic solvents are superimposable with the reference pattern and therefore no polymorphs or solvates can be identified under the studied conditions.

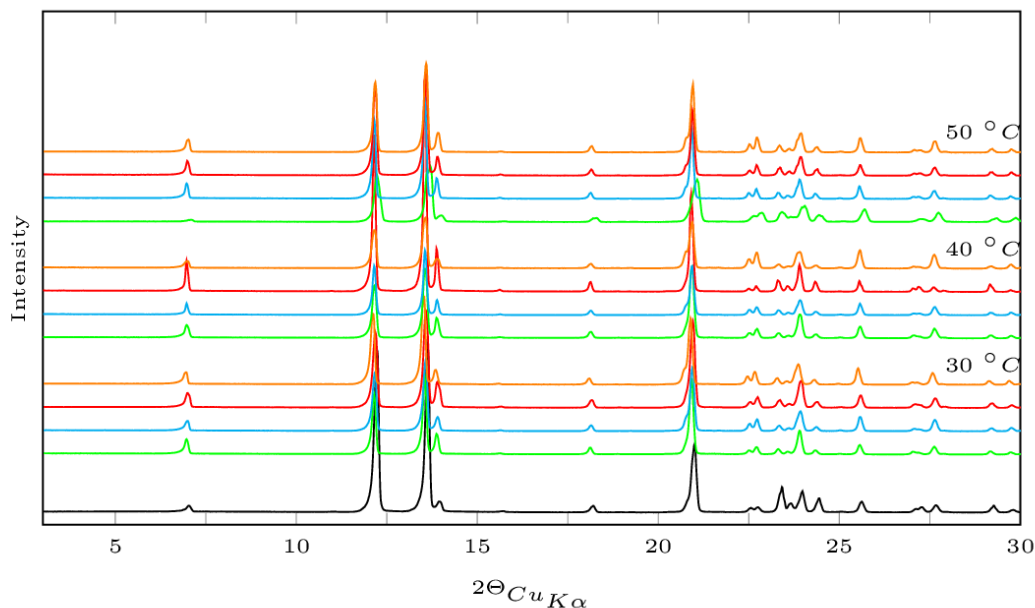


**Fig. 5.** PXRD patterns of the solid excess in equilibrium with the saturated solutions in various organic solvents at three different temperatures. Guaifenesin purchased from TCI Deutschland GmbH is used as reference (black); (orange) ethanol; (red) acetone ;(cyan) 2-propanol; (green) ethyl acetate

#### 4.3. Modelling method and its application to density and solubility data

After thermal and X-ray characterization of guaifenesin, we focus on its solution thermodynamics analysis. In this regard, density and the solubility data are considered. We are looking at the binary solutions of pharmaceuticals and the phase rule dictates that only one degree of freedom exists on the solubility curve at constant pressure. Therefore, we measured the independent density data and used these values as well as the solubility data in order to have a more robust training of the model. In undersaturated solutions, there are two degrees of freedom for a binary solution at fixed pressure. This helps the model to capture the influence of the variation of two independent variables; namely temperature and concentration, on model-specific parameters. There is no PC-SAFT parameters available for guaifenesin, hence we used aqueous solubility and densities of undersaturated solutions of guaifenesin to obtain the model parameters. For ketoprofen and artemisinin we use PC-SAFT

parameters that are reported in the literature [Spy11]. To model the solubility curve of each drug in the respective solvent we use only two solubility data points at the highest and lowest temperature of the solubility range to fit the binary interaction parameter  $k_{ij} = k_{ij,298.15K} + k_{ij,T}(T - 298.15)$ . In this sense, the rest of the solubility curves are pure predictions of the model. All of the model parameters are summarized in Tables 4-7.

**Table 4.** Component specific parameter for PC-SAFT used in this work.

Reference	$\kappa^{A,B_i}$	$\frac{\epsilon^{A,B_i}}{k}$	$\frac{u}{k}$ (K)	$\sigma$ (Å)	m	Component
			(K)			
This work	0.0360	2000.9651	243.9876	2.8441	7.5516	Guaifenesin
[Spy11]	0.0100	1465.5500	298.9600	3.3635	4.6712	Ketoprofen
[Pru14]	0.0200	0.0000	293.7630	2.9590	6.8450	Artemisinin
[Vei20]	0.0451	2425.6700	353.9400	*	1.2047	Water
[Rüt09]	0.0250	2253.9000	208.4200	3.2090	3.0930	Isopropanol
[Rüt09]	0.0320	2653.3840	198.2370	3.1770	2.3830	Ethanol
[Rüt09]	0.0100	0.0000	230.8000	3.3080	3.5370	Ethyl acetate
[Rüt09]	0.0100	0.0000	247.4180	3.2280	2.8910	Acetone
[Vei19]	0.0100	0.0000	311.3100	3.1898	2.3290	Acetonitrile
[Spy11]	1.4000	1220.6100	172.2900	3.1538	3.5904	MEK
[30]	0.0000	0.0000	285.6900	3.7169	2.8149	Toluene

\*:  $\sigma = 2.7927 + 10.11 \cdot \exp(-0.01775 \cdot T) - 1.417 \cdot \exp(-0.01146 \cdot T)$

**Table 5.** Values of  $k_{ij}$  parameter of various solvents and guaifenesin fitted in this work.

$k_{ij,T^2}$	$k_{ij,T}$	$k_{ij,298.15K}$	Solvent
-2.3741E-5	1.0944E-4	-0.0330	Water
0.0000	-1.7521E-4	-0.0034	Isopropanol
0.0000	-1.0596E-4	-0.0208	Ethanol
0.0000	2.2433E-4	-0.0129	Ethyl acetate
0.0000	2.5069E-4	-0.0129	Acetone

**Table 6.** Values of  $k_{ij}$  parameter of various solvents and ketoprofen fitted in this work.

$k_{ij,T}$	$k_{ij,298.15K}$	Solvent
-7.1995E-4	-0.0129	Isopropanol
-6.0916E-4	-0.0289	Ethanol
-1.7882E-4	-0.0089	Ethyl acetate
2.8174E-5	0.0273	Acetonitrile
-1.7977E-4	0.0185	Toluene

**Table 7.** Values of  $k_{ij}$  parameter of various solvents and artemisinin fitted in this work.

$k_{ij,T}$	$k_{ij,298.15K}$	Solvent
-2.3578E-4	-0.0288	Ethanol
-5.2808E-4	-0.0105	Ethyl acetate
-1.2933E-4	0.0521	Acetonitrile
-4.7967E-4	-0.0842	MEK
-3.6881E-4	-0.0122	Toluene

In what follows, we start by looking at the behavior of density of guaifenesin. Then, we systematically investigate the solubility of guaifenesin, ketoprofen and artemisinin in different solvents.

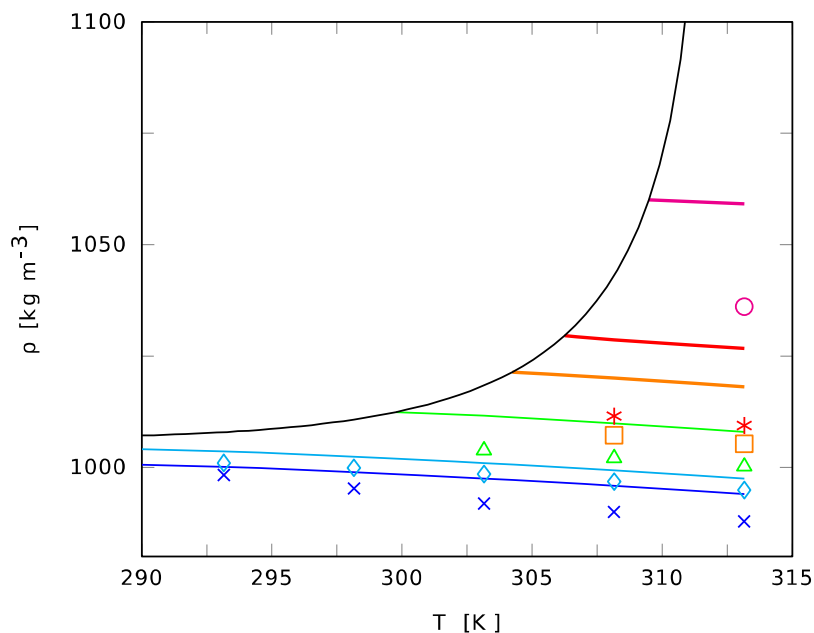
#### 4.3.1. Solid and solution density of guaifenesin

Table 8 shows the results of density measurements of aqueous solutions of guaifenesin at different temperatures. These values alongside with the density line of saturated solutions are depicted in Fig. 6, as well. As this figure shows, density data in the saturated solutions increase with the increase of concentration. This increase is not appreciable until  $\sim 308$  K and after that, the density increases sharply. This is a direct consequence of the solubility behavior of guaifenesin in water as will be discussed in the next chapter. Density data of undersaturated solutions decrease with the increase of temperature and increase with the increase of concentration. Although a slight relative deviation from the experimental data, the model can capture the concentration and temperature variations of the density data. Fitting the solubility and density at the same time makes the density calculations less accurate. However, the model can still be used to represent the solubility data with high accuracy as is shown in the next section.

**Table 8.** Experimentally determined density values of undersaturated aqueous guaifenesin solutions.

313.15	308.15	303.15	298.15	293.15	$T$ [K]
$\rho_{solution} [g\ cm^{-3}]$					$x$ [-]
0.9879	0.9900	0.9919	0.9953	0.9983	0.0005
0.9949	0.9968	0.9985	0.9999	1.001	0.0014
1.0002	1.0021	1.0038			0.0041
1.0053	1.0072				0.0068
1.0094	1.0115				0.0091
1.0361					0.0186

Average standard deviation S.D. =  $0.0002\ g\ cm^{-3}$ .



**Fig. 6.** Density of guafenesin aqueous solutions at different temperatures and saturations. (x, blue) 0.0005 mol%, ( $\diamond$ , cyan) 0.0014 mol%, ( $\Delta$ , green) 0.0041 mol%, ( $\square$ , orange) 0.0068 mol%, (\*,red) 0.0091 mol%, ( $\circ$ , magenta) 0.0186 mol%. Black line: saturation line. Lines are calculated using PC-SAFT.

Also, the density of solid guafenesin,  $\rho_{\text{solid}}$ , was measured as  $1.28 \text{ g cm}^{-3}$  at 303.15 K. Saturated-solution densities,  $\rho_{\text{sat.-solution}}$ , ranging between  $1.0078 \text{ g/cm}^3$  for the aqueous solution and  $0.8094 \text{ g/cm}^3$  in 2-propanol were observed. Densities of non-aqueous solutions are summarized in Table 9. Except the acetone solution, the order of the increases in densities in saturated solutions follow the order of the pure solvent densities.

**Table 9.** Experimentally determined density values of solutions of guafenesin in various solvents, saturated at  $T=303.15 \text{ K}$ .

$\rho_{\text{sat.-solution}} [\text{g cm}^{-3}]$	$T_{\text{cell}} [\text{K}]$	$\omega_{\text{sat.}} [g_{\text{solute}} g_{\text{solution}}^{-1}]$	
0.8438	303.15	0.19	Ethanol

0.8302	303.15	0.17	Acetone
0.8094	303.15	0.11	2-Propanol
0.9004	303.15	0.05	Ethyl acetate

---

### 4.3.2. Solubility data of guaifenesin

The solubility of guaifenesin in several organic solvents was determined exploiting the isothermal method described in the experimental part. The solubility data are given in Table 10 and are graphically represented in Fig. 7.

**Table 10.** Experimental solubility data of guaifenesin in several organic solvents between 283.15 and 333.15 K and related standard deviation (S.D.).

.S.D	$\omega_{sat} . [g_{solute} g_{solution}^{-1}]$	.S.D	$\omega_{sat} . [g_{solute} g_{solution}^{-1}]$	T [K]
Acetone		Ethanol		
0.001	0.066	0.005	0.070	283.15
0.002	0.094	0.002	0.104	293.15
0.004	0.166	0.009	0.194	303.15
0.004	0.295	0.006	0.337	313.15
0.002	0.501	0.012	0.58	323.15
0.056	0.701	0.063	0.751	333.15
Ethyl acetate		Propanol-2		
0.001	0.018	0.001	0.035	283.15
0.003	0.023	0.001	0.057	293.15
0.002	0.047	0.004	0.109	303.15
0.005	0.087	0.002	0.216	313.15
0.005	0.194	0.002	0.413	323.15
0.018	0.451	0.018	0.671	333.15

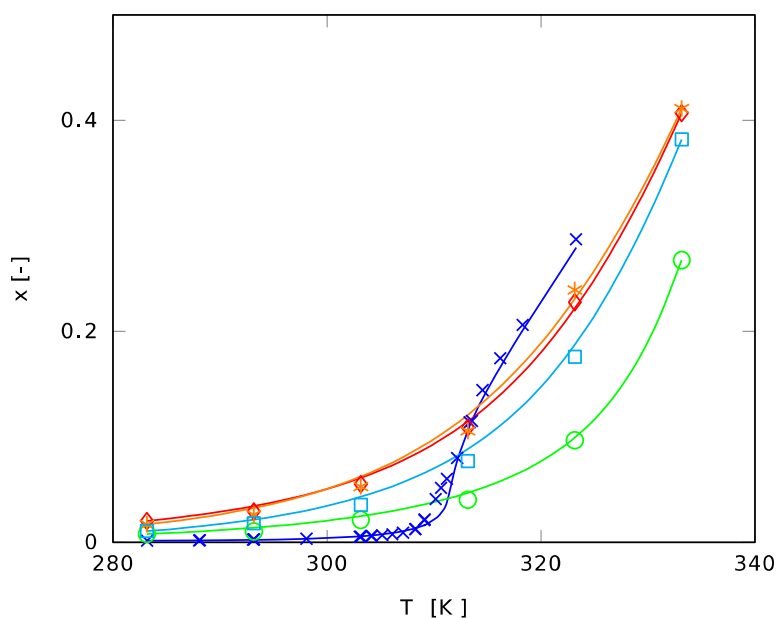


**Fig. 7.** Experimental solubility data in mole fraction,  $x$ , of guaifenesin in several solvents: (x, blue) water; (\*, orange) ethanol; ( $\diamond$ , red) acetone; ( $\square$ , cyan) 2-propanol; ( $\circ$ , green) ethyl acetate. Lines are calculated using PC-SAFT.

The data show that guaifenesin is highly soluble in polar solvents, exhibiting the highest solubility in ethanol followed by acetone, 2-propanol and ethyl acetate in the studied range of temperature. In Fig. 7, we also superimposed our previously reported aqueous solubility of guaifenesin and its solubility in 2-propanol [Cas20]. As already mentioned we used only two solubility data points to obtain the binary interaction parameters between guaifenesin and each solvent. These two data points are the solubility data at the minimum and the maximum temperature in the range of experimental measurements. Therefore, the solubility at other temperatures are predicted using PC-SAFT. Fig. 7 supports that the model describes the solubility curves in a very good agreement with experimental data. Moreover, an increase of solubility with the temperature is clearly observed in all solvents and the model captures the behavior.

Fig. 8 shows the van't Hoff plot of these data sets. The solid line in this figure is the so-called ideal solubility or the activity of solid guaifenesin. The sketches of Fig. 8 show that except at higher temperatures where we approach the melting point of guaifenesin, the data are distinctly different from the ideal solubility line. This shows the non-ideal behavior of the guaifenesin in all of the solvents. Interestingly, most of the data shows a nonlinear trend as well. Therefore, the slopes of these van't Hoff plots are not constant, meaning that the so-called van't Hoff enthalpy of solution changes with the temperature. The difference between the solid line that is the activity of the solid guaifenesin and the markers in Fig. 8 is due to the effect of activity coefficients. It can be seen that all of the solutions behave non-ideally with positive deviations from Raoult's law. The steep increase of the solubility of guaifenesin in water after a certain temperature ( $T \sim 310$  K) is also a direct consequence of the

decrease of its activity coefficients as aqueous data points approaching the solid line steeply with increase of temperature.

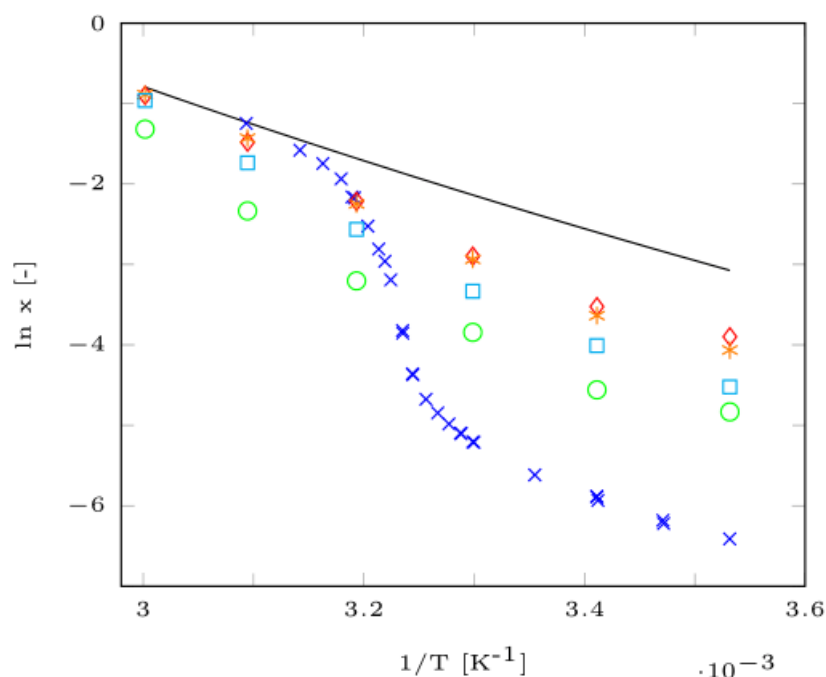


**Fig. 8.** van't Hoff plot of guafenesin solubilities in several solvents: (x, blue) water; (\*, orange) ethanol; ( $\diamond$ , red) acetone; ( $\square$ , cyan) 2-propanol; ( $\circ$ , green) ethyl acetate. Black line: activity of the solid phase calculated using Eq. (4).

To verify our modelling approach, we investigate the solubility modelling of ketoprofen and artemisinin. The solubility data are reported in the literature [Sot20]. As Figs. 9 and 10 show, the model is in good agreement with the experimental data. It should be noted that the ketoprofen data were modelled using purely empirical equations by fitting the model parameters to all of the data points [Sot20]. However, we only use the solubility data at the highest and the lowest temperatures for the fitting and the rest of the curve is prediction.

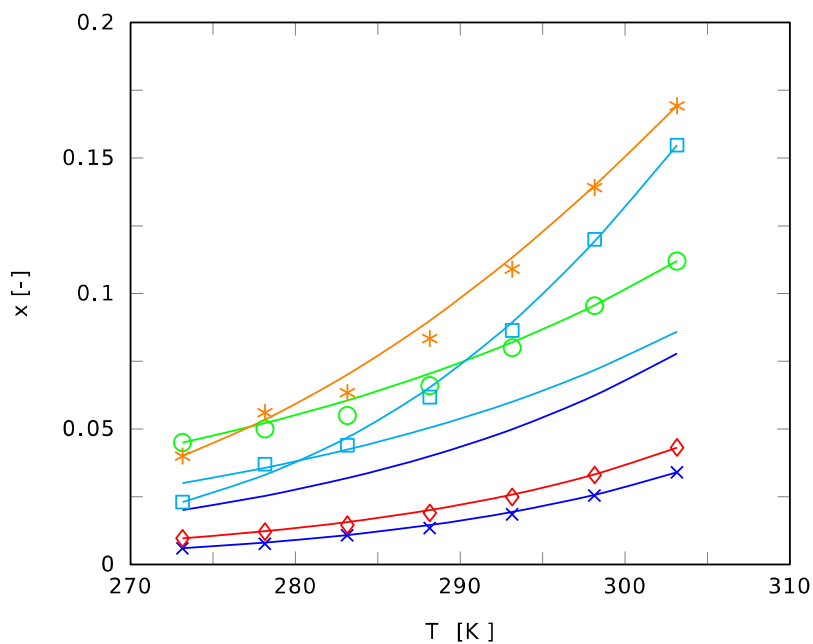


**Fig. 9.** Solubility of ketoprofen in various solvents at different temperatures. (x, blue) toluene; (\*, orange) ethanol; ( $\diamond$ , red) acetonitrile; ( $\square$ , cyan) 2-propanol; ( $\circ$ , green) ethyl acetate. Solid lines are calculated using PC-SAFT. Dashed lines are calculated with  $k_{ij}=0$  .

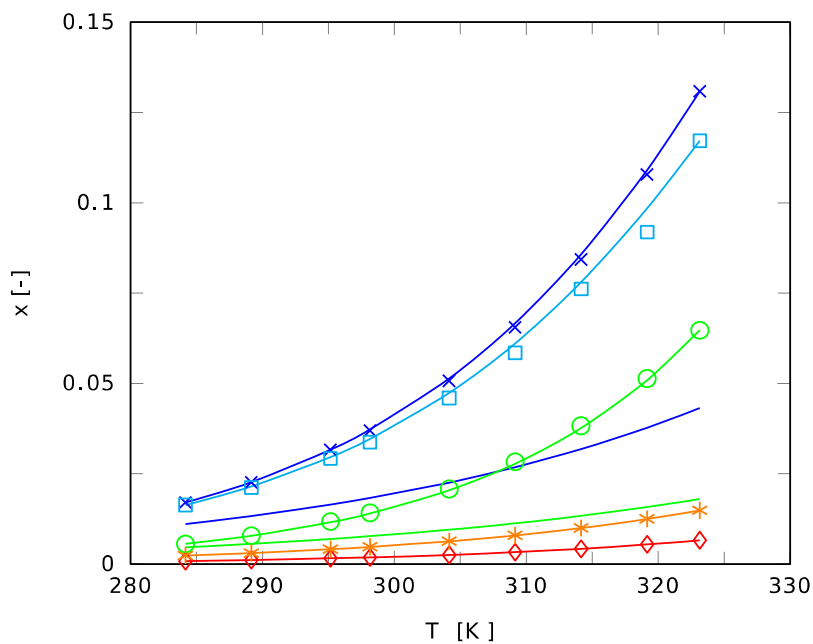


**Fig. 10.** Solubility of artemisinin in various solvents at different temperatures: (x, blue) toluene; (\*, orange) ethanol; ( $\diamond$ , red) acetonitrile; ( $\square$ , cyan) methyl ethyl ketone; ( $\circ$ , green) ethyl acetate. Solid lines are calculated using PC-SAFT. Dashed lines are calculated with  $k_{ij}=0$  .

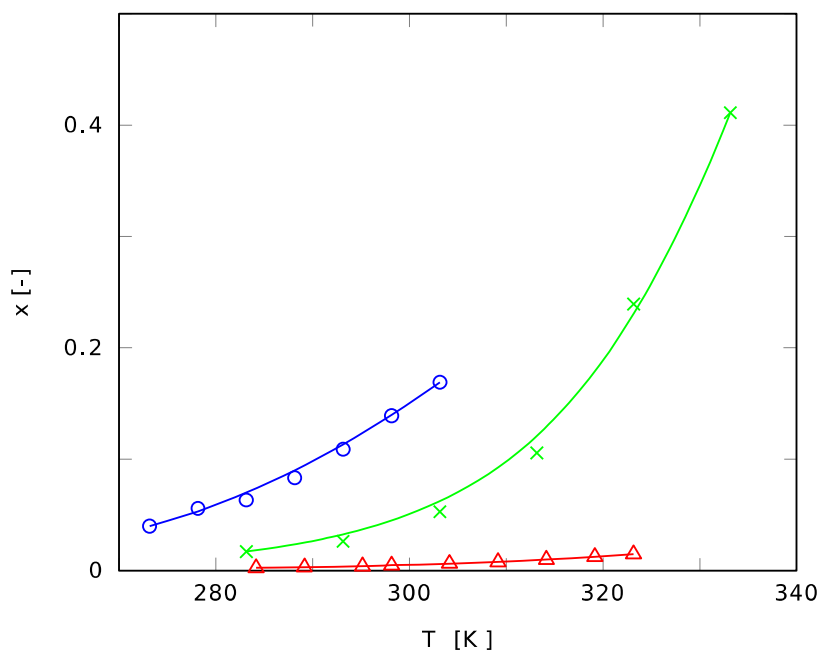


**Fig. 11.** Experimental solubility points of ketoprofen ( $\circ$ , blue), guaifenesin ( $\times$ , green), and artemisinin ( $\Delta$ , red) in ethanol. Lines are calculated using PC-SAFT.

Figs. 9 and 10 also contain the purely prediction of the solubility curves by setting  $k_{ij}=0$ . The predicted curves show that the model is able to distinguish between the effect of the solvents on the solubility of these drugs. Although the prediction differs quantitatively with the experimental data, this is very important in the solvent screening step. This enables the practitioner to choose the right solvent without doing many experimental efforts.

Figs. 11 and 12 exemplarily compare the solubility curves of the three pharmaceuticals in ethanol and ethyl acetate respectively. It can be seen that ketoprofen exhibits highest solubility in both of the solvents investigated, followed by guaifenesin and artemisinin. The model also can describe the experimentally observed behavior.

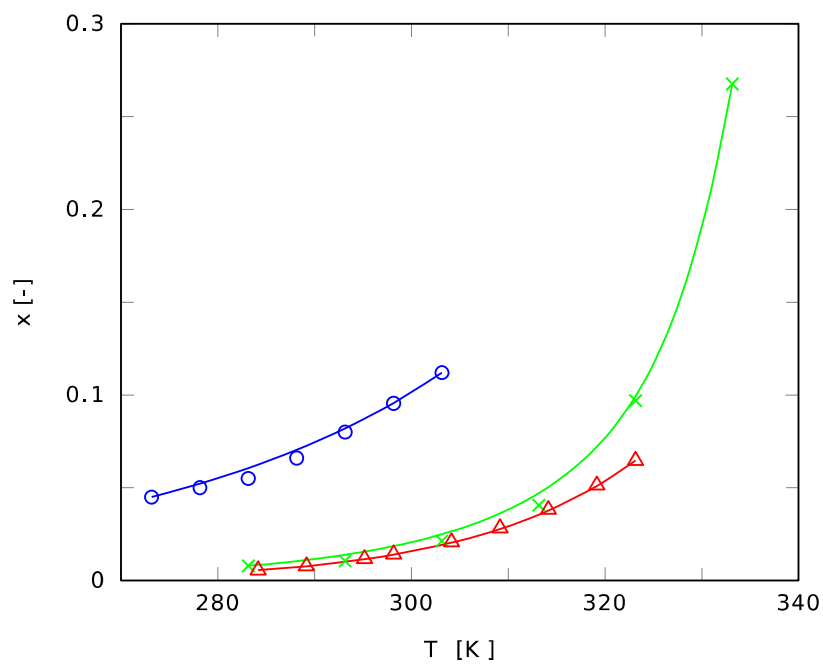


**Fig. 12.** Experimental solubility points of ketoprofen ( $\circ$ , blue), guaifenesin ( $\times$ , green), and artemisinin ( $\Delta$ , red) in ethyl acetate. Lines are calculated using PC-SAFT.

## 5. Conclusions

Thermal analysis and PXRD experiments confirmed that the antitussive agent guaifenesin does not undergo a polymorphic phase transition before it melts. A subsequent systematic investigation of its density and solubility parallel to solubility comparison with other chiral molecule ketoprofen and antimalarial drug artemisinin has been done. PC-SAFT EoS was used to model the data. To capture the temperature and concentration dependence of the data, density measurements of undersaturated aqueous solutions of guaifenesin were used to obtain more robust model parameters. The model is able to represent the solubility behavior of all three drugs in different solvents using only a small amount of data for the fitting of the free parameters. It is also able to capture temperature effects and can well distinguish between the different solutes and solvents. Experimental data showed that guaifenesin is the most soluble in ethanol and least soluble in ethyl acetate. Moreover, in these solvents ketoprofen is the highest soluble followed by guaifenesin and artemisinin. Based on the results of this study we aim to extend the work to evaluate other solutions, especially mixed-solvent systems.

## Acknowledgement

We are grateful to Mrs. Jacqueline Kaufmann and Mrs. Stefanie Oberländer for their help in thermal analysis and PXRD measurements.

## List of symbols

Universal gas constant ( $\text{Pa}\cdot\text{m}^3\cdot\text{mol}^{-1}\cdot\text{K}^{-1}$ )	$R$
Compressibility factor	$Z$
Activity	$a$
Molar enthalpy (kJ/mol)	$H$
Molar heat capacity ( $\text{J}/(\text{K mol})$ )	$C_p$
Mass (g)	$m$
Mole fraction	$x$
Mass solubility ( $\text{g}_{\text{solid}}/\text{g}_{\text{solvent}}$ )	$\omega$
Different molecules $i$ and $j$	$i, j$
Absolute temperature (K)	$T$
Association site A	$A$

	Association site B	<i>B</i>
	Molar mass (g/mol)	<i>M</i>
	Non-Random Two Liquid-Segment Activity Coefficient model	<i>NRTL–SAC</i>
	Universal Quasi Chemical theory	<i>UNIQUAC</i>
	UNIQuac Functional Activity coefficient model	<i>UNIFAC</i>
	Equation of State	<i>EoS</i>
	Perturbed-Chain Statistical Associating Fluid Theory	<i>PC–SAFT</i>
	Dispersion energy parameter (K)	$\frac{u}{k}$
	Fitting parameter accounting for dispersion energy corrections between <i>i</i> and <i>j</i>	$k_{ij}$

### Superscripts

Fusion	fus
Residual	res

### Subscripts

Melting / molar	m
-----------------	---

### Greek letters

Activity coefficient	$\gamma$
Fugacity coefficient	$\phi$
Chemical potential (J/mol)	$\mu$
Segment diameter (Å)	$\sigma$
Association volume parameter	$\kappa$
Association energy parameter (K)	$\frac{\varepsilon}{k}$

### References

- [1] L. Di, P. V. Fish, T. Mano, Bridging solubility between drug discovery and development, *Drug Discovery Today*, 17 (2012) 486-495. <https://doi.org/10.1016/j.drudis.2011.11.007>
- [2] R. Soto, M. Svärd, V. Verma, L. Padrela, K. Ryan, Å. C. Rasmuson, Solubility and thermodynamic analysis of ketoprofen in organic solvents, *Int. J. Pharm.*, 588(2020)119686, <https://doi.org/10.1016/j.ijpharm.2020.119686>

- [3] M. Sadeghi, Å. C. Rasmuson, Solubility of Salicylic Acid, Salicylamide, and Fenofibrate in Organic Solvents at Low Temperatures, *J. Chem. Eng. Data*, 65(2020) 4855–4861. <https://doi.org/10.1021/acs.jced.0c00443>
- [4] M. Lin, M. Tesconi, M. Tischler, Use of H-1 NMR to facilitate solubility measurement for drug discovery compounds, *Int. J. Pharm.*, 369 (2009) 47-52. <https://doi.org/10.1016/j.ijpharm.2008.10.038>
- [5] M. B. Rask, M. M. Knopp, N. E. Olesen, R. Holm, T. Rades, Comparison of two DSC-based methods to predict drug-polymer solubility, *Int. J. Pharm.*, 540(2018) 98-105. <https://doi.org/10.1016/j.ijpharm.2018.02.002>
- [6] M. Yang, P. Wang, H. Suwardie, C. Gogos, Determination of acetaminophen's solubility in poly(ethylene oxide) by rheological, thermal and microscopic methods, *Int. J. Pharm.*, 403 (2011) 83-89. <https://doi.org/10.1016/j.ijpharm.2010.10.026>
- [7] H. He, R. Sun, Y. Wan, J. Sha, L. Yuan, G. Jiang, Y. Li, T. Li, B. Ren, Solubility measurement, thermodynamic correlation and molecular dynamic simulation of naphazoline hydrochloride in four binary solvents, *J. Mol. Liq.*, 323 (2021)114632. <https://doi.org/10.1016/j.molliq.2020.114632>
- [8] M. Sadeghi, Å. C. Rasmuson, On the estimation of crystallization driving forces, *CrystEngComm*, 21(2019) 5164-5173. <https://doi.org/10.1039/C9CE00747D>
- [9] T. A. Reddy, C. Garlapati, Dimensionless empirical model to correlate pharmaceutical compound solubility in supercritical carbon dioxide, *Chem. Eng. & Technol.*, 42(2019) 2621-2630. <https://doi.org/10.1002/ceat.201900283>
- [10] C.-C. Chen, Y. Song, Solubility modeling with a nonrandom two-liquid segment activity coefficient model, *Ind. Eng. Chem. Res.*, 43(2004) 8354–8362. <https://doi.org/10.1021/ie049463u>

- [11] M. Valavi, M. Svärd, Å. C. Rasmuson, Prediction of the solubility of medium-sized pharmaceutical compounds using a temperature-dependent NRTL-SAC model, *Ind. Eng. Chem. Res.*, 55(2016) 11150–11159. <https://doi.org/10.1021/acs.iecr.6b02609>
- [12] M. Mirmehrabi, S. Rohani, L. Perry, Thermodynamic modeling of activity coefficient and prediction of solubility: Part 2. Semipredictive or semiempirical models, *J. Pharm. Sci.*, 95(2006) 798-809. <https://doi.org/10.1002/jps.20576>
- [13] E. Sheikholeslamzadeh, S. Rohani, Solubility prediction of pharmaceutical and chemical compounds in pure and mixed solvents using predictive models, *Ind. Eng. Chem. Res.*, 51(2012) 464–473. <https://doi.org/10.1021/ie201344k>
- [14] F. L. Mota, A. J. Queimada, A. E. Andreatta, S. P. Pinho, E. A. Macedo, Calculation of drug-like molecules solubility using predictive activity coefficient models, *Fluid Phase Equilibr.*, 322-323(2012) 48-55. <https://doi.org/10.1016/j.fluid.2012.02.003>
- [15] B. Bouillot, S. Teychené, B. Biscans, An evaluation of thermodynamic models for the prediction of drug and drug-like molecule solubility in organic solvents, *Fluid Phase Equilibr.*, 309 (2011) 36-52. <https://doi.org/10.1016/j.fluid.2011.06.032>
- [16] A. Diedrichs, J. Gmehling, Solubility calculation of active pharmaceutical ingredients in alkanes, alcohols, water and their mixtures using various activity coefficient models," *Ind. Eng. Chem. Res.*, 50 (2011) 1757–1769. <https://doi.org/10.1021/ie101373k>
- [17] F. Rüther, G. Sadowski, Modeling the solubility of pharmaceuticals in pure solvents and solvent mixtures for drug process design, *J. Pharm. Sci.*, 98(2009) 4205-4215. <https://doi.org/10.1002/jps.21725>

- [18] T. Spyriouni, X. Krokidis, I. G. Economou, Thermodynamics of pharmaceuticals: Prediction of solubility in pure and mixed solvents with PC-SAFT," *Fluid Phase Equilibr.*, 302(2011) 331–337. <https://doi.org/10.1016/j.fluid.2010.08.029>
- [19] A. Klamt, F. Eckert, M. Hornig, M. E. Beck, T. Bürger, Prediction of aqueous solubility of drugs and pesticides with COSMO-RS," *J. Comput. Chem.*, 23 (2002) 275–281. <https://doi.org/10.1002/jcc.1168>
- [20] B. Lee, S. Lin, Prediction and screening of solubility of pharmaceuticals in single- and mixed-ionic liquids using COSMO-SAC model, *AIChE J.*, 63(2017) 3096-3104. <https://doi.org/10.1002/aic.15595>
- [21] P. V. Dicipinigaitis, Y. E. Gayle, G. Solomon, R. D. Gilbert, Inhibition of cough-reflex sensitivity by benzonatate and guaifenesin in acute viral cough, *Respiratory Medicine*, 103(2009) 902-906. <https://doi.org/10.1016/j.rmed.2008.12.008>
- [22] H. M. Maher, S. M. Al-Taweel, M. M. Alshehri, N. Z. Alzoman, Novel stereoselective high-performance liquid chromatographic method for simultaneous determination of guaifenesin and ketorolac enantiomers in human plasma, *Chirality*, 26(2014) 629-639. <https://doi.org/10.1002/chir.22354>
- [23] N. Mani, H. W. Jun, J. W. Beach, J. Nerurkar, Solubility of guaifenesin in the presence of common pharmaceutical additives, *Pharm. Develop. Technol.*, 8(2003) 385-396. <https://doi.org/10.1081/PDT-120024692>
- [24] R. R. Fayzullin, H. Lorenz, Z. A. Bredikhina, A. A. Bredikhin, A. Seidel-Morgenstern, Solubility and some crystallization properties of conglomerate forming chiral drug guaifenesin in water, *J. Pharm. Sci.*, 103 (2014) 3176–3182. <https://doi.org/10.1002/jps.24104>

- [25] F. Cascella, E. Temmel, A. Seidel-Morgenstern, H. Lorenz, Efficient resolution of racemic guaifenesin via batch-preferential crystallization processes, *Org. Process Res. Dev.*, 24(2020) 50–58. <https://doi.org/10.1021/acs.oprd.9b00413>
- [26] T. R. Kommuru, M. A. Khan, I. K. Reddy, Racemate and enantiomers of ketoprofen: phase diagram, thermodynamic studies, skin permeability, and use of chiral permeation enhancers," *J. Pharm. Sci.*, 87(1998) 833-840. <https://doi.org/10.1021/js9704644>
- [27] K. Gilmore, D. Kopetzki, J. W. Lee, Z. Horváth, D. T. McQuade, A. Seidel-Morgenstern, P. H. Seeberger, Continuous synthesis of artemisinin-derived medicines, *Chem. Commun.*, 50(2014) 12652-12655. <https://doi.org/10.1039/C4CC05098C>
- [28] J. M. Prausnitz, R. N. Lichtenthaler and E. G. de Azevedo, *Molecular Thermodynamics of Fluid Phase Equilibria*, 3rd ed., Prentice-Hall, 1999.
- [29] J. Gmehling, M. Kleiber, B. Kolbe and J. Rarey, *Chemical Thermodynamics for Process Simulation*, 2nd ed., Weinheim: Wiley-VCH, 2019.
- [30] J. Gross, G. Sadowski , Perturbed-chain SAFT: An equation of state based on a perturbation theory for chain molecules, *Ind. & Eng. Chem. Res.*, 40(2001) 1244-1260. <https://doi.org/10.1021/ie0003887>
- [31] J. Gross, G. Sadowski , Application of the perturbed-chain SAFT equation of state to associating systems, *Ind. & Eng. Chem. Res.*, 41(2002) 5510-5515. <https://doi.org/10.1021/ie010954d>
- [32] M. S. Wertheim, Fluids with highly directional attractive forces. I. Statistical thermodynamics, *J. Stat. Phys.*, 35(1984) 19–34. <https://doi.org/10.1007/BF01017362>
- [33] M. S. Wertheim, Fluids with highly directional attractive forces. II. Thermodynamic perturbation theory and integral equations, *J. Stat. Phys.*, 35(1984) 35–47. <https://doi.org/10.1007/BF01017363>

- [34] M. Wertheim, Fluids with highly directional attractive forces. III. Multiple attraction sites, *J. Stat. Phys.*, 42(1986) 459–476. <https://doi.org/10.1007/BF01127721>
- [35] M. S. Wertheim, Fluids with highly directional attractive forces. IV. Equilibrium polymerization, *J. Stat. Phys.*, 42(1986) 477–492. <https://doi.org/10.1007/BF01127722>
- [36] W. G. Chapman, K. E. Gubbins, G. Jackson, M. Radosz, New reference equation of state for associating liquids, *Ind. Eng. Chem. Res.*, 29(1990) 1709–1721. <https://doi.org/10.1021/ie00104a021>
- [37] H. Tam Do, Y. Zen Chua, J. Habicht, M. Klinksiek, S. Volpert, M. Hallermann, M. Thome, D. Pabsch, D. Zaitsau, C. Schick, C. Held, Melting properties of peptides and their solubility in water. Part 2: di- and tripeptides based on glycine, alanine, leucine, proline, and serine," *Ind. Eng. Chem. Res.*, 60(2021) 4693–4704. <https://doi.org/10.1021/acs.iecr.0c05652>
- [38] K. Parvaneh, A. Shariati, Quasi-chemical PC-SAFT: an extended perturbed chain-statistical associating fluid theory for lattice-fluid mixtures, *J. Phys. Chem. B*, 121(2017) 8338–8347. <https://doi.org/10.1021/acs.jpccb.7b05483>
- [39] A. P. Carneiro , C. Held, O. Rodríguez, G. Sadowski, E. A. Macedo, Solubility of sugars and sugar alcohols in ionic liquids: measurement and PC-SAFT modeling, *J. Phys. Chem. B*, 117(2013) 9980–9995. <https://doi.org/10.1021/jp404864c>
- [40] P. Krenn, P. Zimmermann, M. Fischlschweiger, T. Zeiner, Modeling highly cross-linked epoxy resins in solvents of different polarities with PC-SAFT," *Ind. Eng. Chem. Res.*, 59 (2020) 5133–5141. <https://doi.org/10.1021/acs.iecr.9b06499>
- [41] K. Padiuszyński, U. Domańska, Thermodynamic modeling of ionic liquid systems: development and detailed overview of novel methodology based on the PC-SAFT, *J. Phys. Chem. B*, 116(2012) 5002–5018. <https://doi.org/10.1021/jp3009207>

- [42] F. M. Vargas, D. L. Gonzalez, G. J. Hirasaki, W. G. Chapman, Modeling asphaltene phase behavior in crude oil systems using the perturbed chain form of the statistical associating fluid theory (PC-SAFT) equation of state, *Energy Fuels*, 23(2009)1140–1146. <https://doi.org/10.1021/ef8006678>
- [43] S. P. Tan, M. Piri, Heat of capillary condensation in nanopores: new insights from the equation of state, *Phys. Chem. Chem. Phys.*, 19(2017) 5540-5549. <https://doi.org/10.1039/C6CP07814A>
- [44] H. Veith, C. Luebbert, G. Sadowski, Correctly measuring and predicting solubilities of solvates, hydrates, and polymorphs, *Cryst. Growth Des.*, 20(2020) 723–735. <https://doi.org/10.1021/acs.cgd.9b01145>
- [45] H. Veith, M. Schleinitz, C. Schauerte, G. Sadowski, Thermodynamic approach for co-crystal screening, *Cryst. Growth Des.*, 19(2019) 3253–3264. <https://doi.org/10.1021/acs.cgd.9b00103>
- [46] S. Zarei Mahmoudabadi, G. Pazuki, A predictive PC-SAFT EOS based on COSMO for pharmaceutical compounds, *Sci. Rep.*, 11(2021) 6405-6422. <https://doi.org/10.1038/s41598-021-85942-8>
- [47] Z. A. Bredikhina, V. G. Novikova, D. V. Zakharychev, A. A. Bredikhin, Solid state properties and effective resolution procedure for guaifenesin, 3-(2-methoxyphenoxy)-1,2-propanediol, *Tetrahedron: Asymmetry*, 17(2006) 3015–3020. <https://doi.org/10.1016/j.tetasy.2006.10.027>
- [48] J. Nti-Gyabaah, K. Gbewonyo, Y. C. Chiew, Solubility of artemisinin in different single and binary solvent mixtures between (284.15 and 323.15) K and NRTL interaction parameters, *J. Chem. Eng. Data*, 55(2010) 3356–3363. <https://doi.org/10.1021/je100125x>

- [49] E. Horosanskaia, A. Seidel-Morgenstern, H. Lorenz, Investigation of drug polymorphism: Case of artemisinin. *Thermochim. Acta*, 578(2014) 74-81. <https://doi.org/10.1016/j.tca.2013.12.019>
- [50] A. Prudic, Y. Ji, G. Sadowski, Thermodynamic phase behavior of API/polymer solid dispersions, *Mol. Pharm.*, 11(2014) 2294–2304. <https://doi.org/10.1021/mp400729x>
- [51] E. Temmel, M. J. Eicke, F. Cascella, A. Seidel-Morgenstern, H. Lorenz, Resolution of racemic guaifenesin applying a coupled preferential crystallization-selective dissolution process-Rational process development, *Cryst. Growth Des.*, 19(2019) 3148–3157. <https://doi.org/10.1021/acs.cgd.8b01660>

## Captions for Figures

**Fig. 1.** Molecular structure of (a): 3- (2-methoxyphenoxy) -propane-1, 2-diol (guaifenesin), (b): 2-(3-benzoylphenyl)-propionic acid (ketoprofen) and (c): artemisinin

**Fig. 2.** Schematic representation of the interaction between guaifenesin (i) in water (j) used for the calculations with PC-SAFT.

**Fig. 3.** DSC curve of guaifenesin showing its melting data

**Fig. 4.** Specific heat capacity of guaifenesin as a function of temperature (blue color for the solid and red color for the melt, dotted lines are added as a guide for the eyes)

**Fig. 5.** PXRD patterns of the solid excess in equilibrium with the saturated solutions in various organic solvents at three different temperatures. guaifenesin purchased from TCI (Deutschland GmbH) was used as reference.(black); (orange) ethanol; (red) acetone ;(cyan) 2-propanol; (green) ethyl acetate

**Fig. 6.** Density of guaifenesin in aqueous solution at different temperatures and saturations. (x, blue) 0.0005 mol%, ( $\diamond$ , cyan) 0.0014 mol%, ( $\Delta$ , green) 0.0041 mol%, ( $\square$ , orange) 0.0068 mol%, (\*,red) 0.0091 mol%, ( $\circ$ , magenta) 0.0186 mol%. Black line: saturation line. Lines are calculated using PC-SAFT.

**Fig. 7.** Experimental solubility data of guaifenesin in several solvents: (x, blue) water; (\*,orange) ethanol; ( $\diamond$ , red) acetone ;( $\square$ , cyan) 2-propanol;( $\circ$ , green) ethyl acetate. Lines are calculated using PC-SAFT.

**Fig. 8.** van't Hoff plot of guaifenesin in several solvents: (x, blue) water; (\*, orange) ethanol; ( $\diamond$ , red) acetone;( $\square$ , cyan) 2-propanol;( $\circ$ , green) ethyl acetate. Black line: activity of the solid phase calculated using Eq. (4).

**Fig. 9.** Solubility of ketoprofen in various solvents at different temperatures. (x, blue) toluene; (\*, orange) ethanol; ( $\diamond$ , red) acetonitrile ;( $\square$ , cyan) 2-propanol;( $\circ$ , green) ethyl

acetate. Lines are calculated using PC-SAFT. Dashed lines are calculated with

$$k_{ij}=0 \text{ .}$$

**Fig. 10.** Solubility of artemisinin in various solvents at different temperatures: (x, blue) toluene; (\*, orange) ethanol; ( $\diamond$ , red) acetonitrile ;( $\square$ , cyan) methyl ethyl ketone; ( $\circ$ , green) ethyl acetate. Lines are calculated using PC-SAFT. Dashed lines are calculated with  $k_{ij}=0$  .

**Fig. 11.** Experimental solubility points of ketoprofen ( $\circ$ , blue), guaifenesin (x, green), and artemisinin ( $\Delta$ , red) in ethanol. Lines are calculated using PC-SAFT.

**Fig. 12.** Experimental solubility points of ketoprofen ( $\circ$ , blue), guaifenesin (x, green), and artemisinin ( $\Delta$ , red) in ethyl acetate. Lines are calculated using PC-SAFT.